

The patch like model of galaxies formation: the virial paradox and core–cusp and missing satellite problems

M. Demiański^{1,2}

1.*Institute of Theoretical Physics, University of Warsaw,
02-093 Warsaw, Poland*

2.*Department of Astronomy, Williams College,
Williamstown, MA 01267, USA*

A. Doroshkevich^{3,4}

3.*Astro Space Center of Lebedev Physical Institute of Russian Academy of Sciences,
117997 Moscow, Russia*

4.*National Research Center Kurchatov Institute,
123182, Moscow, Russia*

(Dated: December 2, 2020)

The patch like model of the hierarchical galaxy formation in the Λ CDM cosmological model with small damping scale is considered. In this model galaxies and clusters of galaxies are identified with rare high density peaks, what suppresses the action of random factors in the vicinity of peaks and makes the process of halos formation more rapid and regular. High concentration of irregular subhalos surrounding the central peaks and their subsequent merging just after formation allows to consider this medium as a mixture of collisionless dispersed dark matter (DM) particles and collisional subhalos. Merging of these subhalos with the central dominating halo is accompanied by tidal destruction of the central cusp, what progressively shallows the density profile and promotes formation of super massive central black holes. The simulations [1–3] provide some quantitative characteristics of these processes.

In the framework of this model we can reproduce the observed correlation of mass and density of virialized galaxies and clusters of galaxies known as the *virial paradox* [4, 5]. These correlations are closely linked with the composition of DM and the shape of the power spectrum of density perturbations what allows to restrict these important properties with already available observations. In particular, these correlations put constraints on the HDM and WDM models and allow to test models of cosmological inflation. We confirm that the missing satellite problem is directly linked with the *virial paradox* and reheating of the Universe which increases temperature and entropy of the baryons, prevents formation of first stars and divides halos into two populations: the first one includes galaxies formed before reheating which are mainly concentrated in the vicinity of the massive ones while the second population – numerous dark halos formed after reheating — accumulates majority of DM but does not contain stars. Their spatial distribution is more homogeneous.

INTRODUCTION

During the last decade much progress has been achieved in observations of the cosmic microwave radiation (WMAP and Planck missions, [6, 7], see also [8]) and in simulations of the Large Scale Structure of the Universe, DM halos, galaxies and clusters of galaxies. Many recent reviews [9–19] present various aspects of these processes.

Now the main attention is concentrated on evolution of the baryonic matter and formation of observed luminous galaxies [15, 20–26]. However a few fundamental problems of galaxy formation remain unsolved and are now actively discussed. First of all these are the core–cusp and missing satellites problems. These problems arise when one compares the observed galaxies and the present day simulated DM halos. In the last few years unexpected discovery of the ultra diffuse galaxies [27], galaxies with a deficit of DM component [28, 29] and a

progress in understanding of the Ly- α forest [4, 30–32] complicates the problem of DM – baryons interconnection.

Present day high resolution simulations provide several representative samples of DM halos ranging from dwarf galaxies and up to rich clusters of galaxies. In majority of simulations [1–3, 33, 34] the DM density profile near the center of halos can be characterised as cusp–like and is often approximated by a simple power law:

$$\rho(r) \propto \rho_0/r^\alpha, \quad 1.5 \geq \alpha \sim 1. \quad (1)$$

This profile reproduces reasonably well the observed one in clusters of galaxies. However in less massive galaxies the density profile is more shallow [35–37] and is usually described by more complex expressions [34].

This is the core-cusp problem. After 20 years of study discrepancies between models of CDM universe and observations of low mass galaxies are still pronounced.

Now many models attempt to explain this problem. It has been suggested that the core-cusp conflict could be

resolved by fluctuations of the inner gravitational potential. The most popular explanation of these fluctuations relies on sudden removal of gas from centers of cuspy DM halos caused by energy injected by supernovae [38, 39]. Progressive disruption of the DM cusp owing to its tidal interaction with the gaseous clouds, stars and protostars is discussed in [40–43]. In [44] erosion of the cusp is related to accretion of suitable spherical DM shells.

Of course, these factors lead to some cusp erosion, but a correct estimate of their efficiency is lacking. Recent analysis [16, 45] indicates insufficient variety of mass profiles to explain the observed diversity of dwarf galaxy rotation curves. In turn recent models [44] require a very special kind of DM accretion and conformity between masses of the cusp and the shells.

Another possibility is to use a more complex dark matter model. It remains an open possibility that these tensions may point to exotic particle physics. Such models – the scalar field dark matter, Bose – Einstein condensate, or ultralight axion DM [46, 47] are identical to the CDM model at cosmological scales but differ at galactic scales. All these problems are also reviewed in [19] with more attention put on exotic particle physics.

However the simplest and the most promising models of the cusp disruption were discussed in [1–3, 48, 49] where it was shown that the cusp becomes shallower in the earlier formed low mass DM halos owing to merging of subhalos. This means that the core–cusp problem is mostly a result of insufficient resolution of present day simulations and it disappears in CDM models with a sufficiently small dissipative scale.

In the standard Λ CDM model gravitationally bound DM structures build up hierarchically by a combination of accretion of the diffused surrounding matter and continuous absorption of smaller surrounding halos [17, 19–23, 34]. During the period of mildly nonlinear matter evolution the formation of structure elements is driven by the random velocity field, and at all redshifts it leads to significant matter concentration in filaments and sheets [50–57]. These elements of the structure represent the intermediate asymptotic of the matter condensation and are observed as the Large and Super Large Scale Structure [55]. Later on some fraction of remaining loosely distributed matter is accumulated into compact halos. Formation of DM halos is well described by the Press–Schechter model (PS) [58–60, 62]

In this paper we reconsider the process of DM halos formation in the framework of the Λ CDM model with the power spectrum of density perturbations with a small damping scale [63]. In this model galaxies are associated with the very rare random highest peaks of density perturbations surrounded by many smaller peaks in the immediate vicinity of the central one. These special features lead to a very rapid regular growth of mass of the main halo and progressive tidal disruption of both the absorbed subhalos and the central cusp.

This is the patch like process of formation of massive DM halos when at high redshifts the active creation of new halos is concentrated only in the vicinity of the central peak. Later on at $z \leq 10$ many DM halos are formed in all of space. This model preserves the main features of the usually discussed models of galaxy formation and the large scale matter distribution but the internal structure of early formed halos is more shallow.

Owing to limited resolution, the early period of halos formation at $z \geq 10$ is poorly reproduced by present day simulations [1–3, 34] and for qualitative estimates we have to rely on the Press–Schechter approach [3, 58–60, 62]. Such analysis emphasises the important impact of the shape of the power spectrum and rapid formation of halos at high redshifts $z \geq 10$. It also illustrates a very important role of merging of earlier formed subhalos. Traces of these processes are seen in some present day simulations and are discussed in [12, 17, 64].

As was shown in [5] for objects with virial masses $10^6 M_\odot \leq M_{vir} \leq 10^{14} M_\odot$ the virial density is a regular function of the mass. For galaxies this correlation is traced up to redshift $z \sim 4$ [4], but it fades for both the observed and simulated low mass DM halos [4, 5]. This property of DM halos – the virial paradox – is also reproduced by the considered model and allows to restrict the shape of the small scale power spectrum. It can be useful for discussion of the cosmological inflation and puts restrictions on the WDM models with light DM particles.

Thus considered here patch like model provides satisfactory description of the observed Universe and attenuates differences between properties of the observed and simulated matter distributions. It leads to a more shallow internal structure of halos, introduces differences between galaxies and later formed dark halos and thereby explains both the virial paradox and the missing satellite problem. Simple limited versions of this model have been simulated in [1–3, 48, 49, 65–67]. Further progress can be achieved with special more refined and representative simulations [34, 57].

This paper is organized as follows: the basic properties of the PS and Zel’dovich approaches are discussed in Sec. 2 & 3, some aspects of the process of halos formation in the patch like model are discussed in Sec. 4. Conclusions can be found in Sec. 5. Statistical characteristics of the Zel’dovich approach are presented in the Appendix.

2. BASIC PARAMETERS OF THE Λ CDM MODEL

The standard Λ CDM model assumes the isotropic matter expansion with the Hubble constant H_0 , adiabatic density perturbations with the Harrison – Zel’dovich primordial power spectrum $P(k)$, the dimensionless densities of dark energy, Ω_Λ , dark matter, Ω_{DM} and baryonic matter, Ω_b . The density of nonrelativistic matter, DM,

and baryons together, is determined as $\Omega_m = \Omega_{DM} + \Omega_b$. Observations of Planck [7] allowed to measure these parameters with high precision

$$H^2 = H_0^2[(1+z)^3\Omega_m + \Omega_\Lambda], \quad H_0 \simeq 67.8 \text{ km/s/Mpc},$$

$$\Omega_\Lambda \simeq 0.72, \quad \Omega_{DM} \simeq 0.24, \quad \Omega_b \simeq 0.04, \quad \Omega_m = 0.28. \quad (2)$$

Here z denotes the redshift and the density of nonrelativistic matter is

$$\langle \rho_m \rangle = 33(1+z)^3 \Theta_m M_\odot / \text{kpc}^3, \quad \Theta_m = \Omega_m / 0.28. \quad (3)$$

For this model the growth of perturbations in the linear theory can be approximately described as

$$D(z \geq 1) \approx \frac{1.3}{1+z}. \quad (4)$$

This simple fit [61] is reasonably accurate for the more interesting case $z \geq 1$. More refined expression normalized by the condition $D(0) = 1$ can be found in [62].

2.2 Characteristics of the random density and velocity fields

In this paper we consider the power spectrum with the Harrison – Zel'dovich asymptotic, $P(k) \propto k$, at $k \rightarrow 0$, and CDM-like transfer function, $T^2(k)$, introduced in [68]

$$P(k) = \frac{A^2}{4\pi} l_0^4 k T^2(k l_0) D_w(k l_D), \quad (5)$$

$$l_0 = \frac{Mpc}{\Omega_m h^2} \simeq \frac{7.14}{\Theta_m} Mpc, \quad M_0 = \frac{4\pi}{3} \langle \rho_m \rangle l_0^3 \simeq \frac{5 \cdot 10^{13} M_\odot}{\Theta_m^2}.$$

$$T(x) = \ln(1 + 2.34x) / 2.34x / \epsilon(x) \quad (6)$$

$$\epsilon^4(x) = 1 + 3.89x + (16.4x)^2 + (5.46x)^3 + (6.71x)^4$$

Here k is the comoving wave number and A is the dimensionless amplitude of perturbations. The damping function D_w and the damping scale, l_D , describe damping of perturbations owing to the random motions of DM particles. According to [63] (see also [69]) for DM particles with mass $M_{DM} = 100 \text{ GeV}$ the damping mass M_D can be taken as

$$M_D \simeq \frac{4\pi}{3} \langle \rho_m \rangle l_D^3 \sim 10^{-5} M_\odot.$$

The damping functions D_w depends on properties of the DM particles. Here we assume that the spectrum terminates at $k l_0 \simeq 10^{-4}$, $M_D \simeq 50 M_\odot / \Theta_m^2$.

For the power spectrum (5) the dispersion of the density perturbations is divergent and it is measured in units

of σ_8 which is the relative density perturbation, $\delta\rho/\langle\rho\rangle$, in a sphere of radius $R_8 = 8h^{-1} \text{ Mpc} = 1.6l_0$,

$$\sigma_8^2 = \int_0^\infty d^3k P(k) W^2(R_8 k) \approx \frac{A^2}{236} = 0.64, \quad (7)$$

$$A \approx 12, \quad W(x) = 3(\sin x - x \cos x) / x^3.$$

Here, $W(Rk)$ is the Fourier transform of the real space top-hat filter corresponding to a sphere of radius R and mass $\mu = M/M_0$.

In this model the amplitudes of random velocity, σ_u , and random displacement, σ_s , are

$$\sigma_s^2 = \int_0^\infty d^3k P(k) / k^2 \approx (1.8l_0)^2,$$

$$\sigma_s \simeq 13 \text{ Mpc}, \quad \sigma_u = H_0 \sigma_s \simeq 900 \text{ km/s}. \quad (8)$$

3. THE PRESS–SCHECHTER AND ZEL'DOVICH MODELS OF STRUCTURE FORMATION

The most popular description of evolution of perturbations is the linear theory, discussed in many publications. Unfortunately nonlinear studies of matter condensation can be described analytically only for special cases. In spite of the limited applicability of these models they allow to describe and illustrate the action of some factors that are important for the structure formation and evolution.

3.1 The extended Press – Schechter model

Evolution of spherical compact high density objects – DM halos, galaxies and clusters of galaxies – can be approximated by the Press–Schechter (PS) model [58–60]. This model considers the successive spherical halo formation around random density peaks. It assumes the Gaussian distribution function for the masses accumulated in a spherical volume of radius R with dispersion

$$\sigma_m^2(\mu) = \int_0^\infty d^3k P(k) W^2(kR), \quad \mu = \frac{4\pi \langle \rho_m \rangle R^3}{3M_0}. \quad (9)$$

Formation of halos is determined by the condition

$$D(z) A_{rnd} \sigma_m(M) = 1.686, \quad 1+z \simeq 0.77 A_{rnd} \sigma_m(\mu). \quad (10)$$

Here the function $D(z)$ is given by (4) and $A_{rnd} \geq 0$ characterizes the random height of separate peaks. Its distribution is described by the Gaussian function

$$dW = \sqrt{2/\pi} \exp(-A_{rnd}^2/2) dA_{rnd}.$$

For the spectrum (5) with the transfer function from (6) and $M_D \leq M_\odot$ the important function $\sigma_m(\mu)$ can be fitted by the expression

$$\sigma_m(\mu) \simeq \frac{3\mu^{-0.06}}{1 + 1.82\mu^{0.24}}. \quad (11)$$

The redshift evolution of the fraction of compressed matter, $f_m(z, M)$, is given by [60, 62]

$$\frac{df_m(z, M)}{dM} = 0.37 \frac{dy}{dM} \exp(-y^2) [1 + 0.81/y^{0.6}], \quad (12)$$

$$f_m(z, M_{min}) = 0.18\Gamma(0.5, y_{mn}) + 0.144\Gamma(0.2, y_{mn}),$$

$$y(z, M) \simeq 1./D(z)/\sigma_m(\mu), \quad y_{mn} = y(z, M_{min}).$$

Here $M_{min} \leq M \leq \infty$, $\Gamma(\beta, x)$ is the incomplete gamma function. For $y_{mn} \simeq 0.25(1+z)\mu_{min}^{0.06} \ll 1$, we get

$$f_m \simeq 1 - 0.27y_{mn} - 0.65y_{mn}^{0.4} + \dots \quad (13)$$

For small M_{min} this fit correctly describes the function f_m for $1+z \leq 10$. For the mean mass of a halo we have

$$\langle M(z, M_{min}) \rangle = \frac{1}{f_m(z, M_{min})} \int_{M_{min}}^{\infty} M df_m. \quad (14)$$

3.2 The Zel'dovich model

The first analytic theory of structure formation was provided by the Zel'dovich approximation [50–52]. This theory correctly describes the early anisotropic stage of matter condensation and formation of elements of the Large Scale Structure (LSS) of the Universe – network of filaments and walls–Superclusters (Zel'dovich pancakes) [51–56, 61]. At all redshifts these elements are formed in the course of mildly nonlinear self similar process of matter condensation.

In the Zel'dovich approximation the Eulerian, r_i , and the Lagrangian, q_i , coordinates of particles (fluid elements) and their velocities are related by

$$r_i = (1+z)^{-1} [q_i - D(z)S_i(\mathbf{q})], \quad (15)$$

$$v_i = dr_i/dt = H(z)(1+z)^{-1} [q_i - D(z)\beta(z)S_i(\mathbf{q})],$$

$$\beta(z) = 1 - d \ln D(z) / d \ln(1+z).$$

Here the Lagrangian coordinates of a particle, q_i , are its unperturbed coordinates in the real space, $r_i(z=0) = q_i$, v_i is its velocity, and the random vector $S_i(\mathbf{q})$ characterizes the displacement of a particle from its unperturbed position. The function $D(z)$ is given by (4).

The statistical aspects of this theory had been discussed in [51, 53, 55, 61, 70, 72] and are briefly presented in the Appendix. The random displacement of a particle $S_i(\mathbf{q})$ is described by the Gaussian distribution function with the correlation functions

$$\Psi_{ij}(q) = \frac{\langle S_i(\mathbf{q}_1)S_j(\mathbf{q}_2) \rangle}{\sigma_s^2} = \int_0^\infty dk \frac{k_i k_j}{k^2} \frac{P(k)W(kq)}{\sigma_s^2} \quad (16)$$

$$\Psi_{ij}(q) = \frac{1}{3}\delta_{ij}G_1(q) + \frac{q_i q_j}{3}G_2(q), \quad \Psi_{ij}(0) = \frac{1}{3}\delta_{ij},$$

$$G_1(q) = \frac{4\pi}{\sigma_s^2} \int_0^\infty dk W(qk)P(k), \quad G_2(q) = \frac{dG_1(q)}{dq}.$$

Here $q_i = (\mathbf{q}_1 - \mathbf{q}_2)_i$, $q = |\mathbf{q}_1 - \mathbf{q}_2|$, $W(x)$ is the filter function (7), σ_s is the dispersion of displacement (8). For the power spectrum (5) these functions are fitted by

$$g_{12} = \frac{G_1(q) - 1}{q^2 G_2(q)} \simeq 0.5(1 + 0.43\mu^{1/4} + 0.46\mu^{0.04}),$$

$$G_2(q) \simeq -\frac{0.546\mu^{-0.127}}{1 + 3.86\mu^{0.34}} = -\frac{\sigma_m^2}{5} G_{sm}^2, \quad (17)$$

$$G_{sm} \simeq 1 + 0.16\mu^{0.17} + 0.16\mu^{0.03},$$

where σ_m and the dimensionless mass μ are given by (9). These relations emphasize the close link between the evolutionary rate in the Zel'dovich theory and the PS model.

The Zel'dovich approach emphasizes the strong impact of the anisotropic compression and allows to characterize evolution of the Large Scale Structure rather than formation of distinct DM halos.

3.3 Angular momentum of DM halos

The Zel'dovich theory predicts an asymmetrical collapse what decreases the matter compression and generates the angular momentum for both the separate particles and for halos as a whole. This problem was discussed in [53, 61, 71–77].

The corresponding components of the velocity are characterized by the functions

$$u_i(\mathbf{q}) = H(z)e_{ijk}q_j S_k(\mathbf{q}), \quad (18)$$

$$H^{-2}\langle u_1(\mathbf{q})u_1(\mathbf{p}) \rangle = (q_2 p_2 + q_3 p_3)G_1 + (q_2 p_3 - q_3 p_2)^2 G_2,$$

$$H^{-2}\langle u_1(\mathbf{q})u_2(\mathbf{p}) \rangle = -q_2 p_1 G_1 + (q_1 p_3 - q_3 p_1)(q_3 p_2 - q_2 p_3)G_2,$$

$$G_1 = G_1(|\mathbf{p} - \mathbf{q}|), \quad G_2 = G_2(|\mathbf{p} - \mathbf{q}|),$$

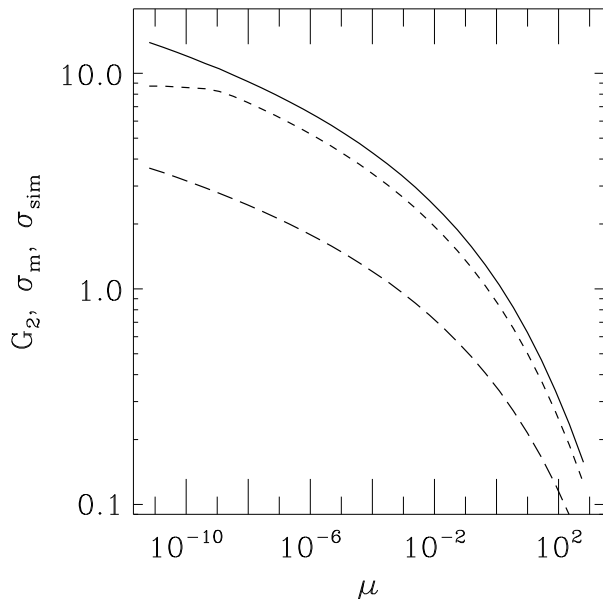


FIG. 1: For spectrum (5) the functions σ_m , with $\mu \geq 10^{-11}$, and $\mu \geq 10^{-9}$, and function $\sqrt{-G_2}$ are plotted vs. dimensionless mass μ by solid, dashed and long dashed lines.

and similar relations for other indexes. The angular momentum of one particle is described as

$$\mathbf{p} = \mathbf{q}, \quad p \ll l_0, \quad u^2(q) \propto 2q^2. \quad (19)$$

The angular momentum of a halo is mainly determined by an even part of the functions (18) and we get

$$J_1^2 \simeq H^2 \int d^3q d^3p (q_2 p_3 - q_3 p_2)^2 G_2. \quad (20)$$

4. PATCH LIKE GALAXY FORMATION IN THE Λ CDM MODEL

In the standard Λ CDM model a gravitationally bound DM structure is built up hierarchically by a combination of accretion of the diffuse surrounding matter and sequential merging of subhalos [17, 20–23, 34, 64]. In the Λ CDM model with a small damping scale galaxies can be identified with the very rare high density peaks while between them the low amplitude perturbations evolve in the linear regime. This difference results in a patch-like galaxy formation which is operating up to small redshifts. It is observed as concentration of denser low mass satellites around massive galaxies and domination of less dense and massive dark DM halos in voids.

The massive halos accumulate many less massive subhalos, which could contain in turn smaller subhalos. High concentration of subhalos near the highest peaks accelerates their merging as compared with accretion of the dispersed DM particles. In turn tidal interactions of the merged loose subhalos with the central cusp of the major halos leads to destruction of subhalos, flattening of the

cusp [1–3, 49, 64] and facilitates formation of super massive black holes. Efficiency of these random processes depends upon the peak amplitude: it is high at high redshifts and decreases with time. On the basis of the present-day simulations the process of halos formation, the important role of subhalos, their tidal disruption and heating etc. are discussed in [12, 17].

Unfortunately, only very complex modern simulations [34] can describe evolution of a box $L \geq 10 Mpc$ with mass resolution $M_{min} \leq M_\odot$ but with only moderate number of halos formed at redshifts $z \geq 10$. Thus to study evolution of DM halos we have to rely on the Press–Schechter formalism and compare its predictions with numerical simulations [1–3].

4.1 Characteristics of relaxed halos

In spite of active discussions the adequate description of the violent relaxation of DM halos is not yet available. Detailed dynamical analysis of this process was performed in [78, 79] for slightly perturbed spherical clouds. The density profile (1) with

$$\alpha \simeq 1.8 - 2,$$

was found in both publications. However this result has a very limited applicability as the spherical collapse is very rare [53]. At high redshifts the simulations [1–3, 49] prefer the density profile with $\alpha \simeq 1.5$.

Efficient method of identification of the distinct virialized elliptical halos has not been proposed yet. The popular phenomenological description of the virial density

$$\rho_{vir} \simeq 18\pi^2 \langle \rho(z) \rangle \simeq 6.6 \cdot 10^3 (1+z)^3 M_\odot / kpc^3, \quad (21)$$

provides rough estimate for spherical systems, but it overestimates ρ_{vir} for the most abundant elliptical systems.

The estimate (21) is based on two assumptions. Firstly, according to [80, 81], collapse of a spherical dust cloud at rest of radius R_0 and density ρ_0 with conservation of mass, M , and energy, E , results in a virialized state

$$E = -\frac{3}{5}G\frac{M^2}{R_0} = \frac{1}{2}U = -\frac{3}{5}G\frac{M_{vir}^2}{2R_{vir}}.$$

Here U is the potential energy of the halo and, therefore,

$$R_{vir} = R_0/2, \quad \rho_{vir} = 8\rho_0. \quad (22)$$

Secondly, at the moment of collapse of the homogeneous spherical halo its average density exceeds the mean cosmological density by a factor

$$\rho_0 / \langle \rho(z) \rangle = 4.5\pi^2.$$

[82] what in combination with (22) results in expression (21).

This estimate remains correct for the Tolman model of evolution of a spherical dust cloud [83], but for deviations from spherical symmetry, such as ellipsoidal deformations [84–87], the energy E decreases with compression of DM. The kinetic energy of rotation and turbulent motions also decrease the expected density (21). Thus the expression (21) can be considered only as *an approximate phenomenological estimate of the complex process of relaxation of collisionless DM*. Owing to its approximate character the coefficient 500 is often used in expression (21) instead of the model coefficient $18\pi^2$.

Moreover the expression (21) leads to an unexpected inference that the virial density depends only upon redshift and, therefore, it is the same for all halos at a given redshift. The wide variety of observed and simulated relaxed halos at $z \leq 1$ indicates that the actual situation is more complex, and it is necessary to restrict such universality. For this purpose it is convenient to introduce the redshift of halo formation, z_{cr} [88] and to use (21) with z_{cr} . Such modified version of (21) agrees with the model of Lacey and Cole [82]. Thus the noted above replacement of factors $18\pi^2$ by 500 implies introduction of redshift of halo formation as

$$(1 + z_{cr})^3 = 2.5(1 + z)^3.$$

Next problem is the correct determination of the shape and boundary of galaxies and clusters [53, 84–90] and determination of halos density in observations and simulations. Thus, very detailed analysis of halos evolution [62] is performed without consideration of possible anisotropy of matter distribution. This factor is specially important for earlier halos, which often resemble to flattened ellipsoids (Zel’dovich pancakes) [53]. Dependence of the halo parameters upon its internal structure [91–93] and/or complex environment [94] should be discussed separately (see, e.g. [15]).

4.2 DM halos as counterparts of galaxies

Some information about the process of galaxy formation can be obtained using the standard technique developed for the description of evolution of random density and velocity fields [3, 51–55, 61, 68, 70]. In order to identify density peaks with galaxies and clusters of galaxies we can compare their mean number densities $\langle n_{cls} \rangle$ and $\langle n_{pk} \rangle$.

In the SDSS for the observed clusters of galaxies with $M_{cls} \geq 10^{13} M_\odot$ the mean number density $\langle n_{cls} \rangle$ and the mean cluster separation, $\langle d_{cls} \rangle$ are estimated as [95]

$$\langle n_{cls} \rangle \sim 10^{-5} Mpc^{-3}, \quad \langle d_{cls} \rangle \sim 45 Mpc \sim 6l_0. \quad (23)$$

In turn for the power spectrum (5) the mean number density of high peaks is determined by the scale l_0 . This

means that clusters are associated with only a small fraction of the high density peaks.

As was shown in [68] the cumulative number density of high peaks of a random scalar field can be roughly estimated as

$$\langle n_{pk} \rangle \simeq \frac{10^{-2}}{l_0^3} \exp\left(-\frac{A_{rnd}^2}{2}\right) \simeq n_{cls}, \quad (24)$$

where A_{rnd} is the peak amplitude. This means that clusters with parameters (23) are identified with the peaks of amplitude

$$A_{rnd} \sim \sqrt{2 \ln(\langle n_{pk} \rangle / \langle n_{cls} \rangle)} \simeq 1.4. \quad (25)$$

For comparison, assuming cosmological origin of Super Massive Black Holes, we can estimate the corresponding peak amplitude for $M_{BH} \sim 10^{10} M_\odot$ as [96–98]

$$n_{BH} \sim 3 \cdot 10^{-9} Mpc^{-3}, \quad A_{rnd} \simeq 4.2. \quad (26)$$

For galaxies the random amplitude A_{rnd} can be estimated from (10) and the assumption that the reionization of the Universe at redshifts $1 + z \sim 10$ is caused by halos with mass $M \sim 10^6 M_\odot$, $\mu \sim 2 \cdot 10^{-8}$. These parameters correspond to $\sigma_m(\mu) \sim 0.7 - 0.8$ and thus $A_{rnd} \sim 1 - 1.2$. More accurate estimate of the peak’s amplitude associated with galaxies – $A_{rnd} \simeq 1 - 2$ will be given in the next subsection.

Of course, this picture predicts formation of many low mass halos in the vicinity of the main halo in a wide range of scales. This successive formation of many low mass DM subhalos continues up to small redshifts. In turn, large scale perturbations regulate the spatial distribution of low mass halos, provide their higher concentration in the immediate vicinity of the central peak and regulate the further transformation of the system of subhalos into the distinct massive objects – galaxies, filaments or sheet-like superclusters.

4.3 The virial density of galaxies and clusters of galaxies: the virial paradox

As was discussed in [5] for galaxies and clusters of galaxies the virial density, ρ_{vir} , is a regular function of their mass. Thus for the sample of 194 observed galaxies and 447 clusters of galaxies with $10^6 \leq M_{vir}/M_\odot \leq 10^{14}$ the reduced virial density G_ρ is fitted as follows:

$$G_\rho^{obs}(\mu) = \frac{\rho_{vir} \sqrt{\mu}}{\langle G_\rho \rangle} \simeq \frac{40\mu^{0.25}}{(1 + 2\mu^{0.25})^3}, \quad (27)$$

$$\langle G_\rho \rangle = 6 \cdot 10^5 M_\odot / kpc^3 \simeq 2 \cdot 10^4 \langle \rho_m(0) \rangle.$$

The maximal value $G_\rho^{obs} \sim 3$ is achieved for $\mu \sim 4 \cdot 10^{-3}$, $M \sim 2 \cdot 10^{11} M_\odot$. In Fig. 2 the function G_ρ^{obs} is plotted

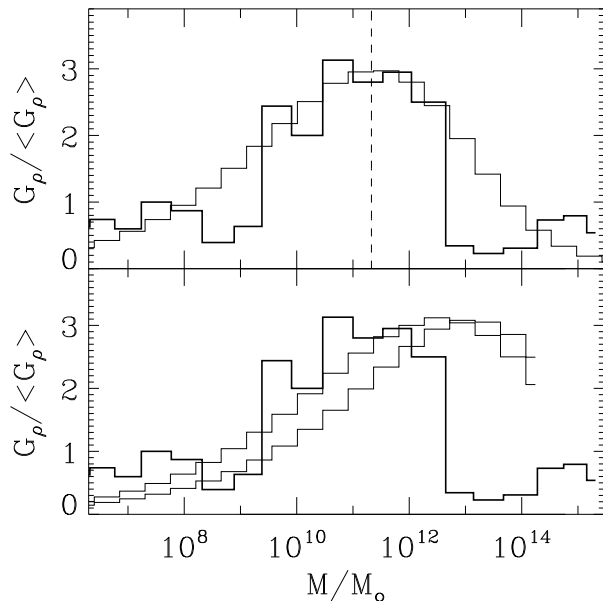


FIG. 2: Top panel: the observed PDF of reduced virial density $G_\rho^{obs}(\mu)$ (27) is plotted by solid line vs. virial mass of halo M/M_\odot . Theoretical function $G_\rho^{th}(\mu)$ (32) is plotted by thin line, dashed line marks the position of maximum. Bottom panel: the same observed PDF G_ρ^{obs} is compared with the PDFs (29) and PDF, for function $\sigma_m(M)$ presented in [62].

vs. virial mass of halos M_{vir}/M_\odot . More detailed analysis of several clusters [84–87] confirms this estimate [5].

The corresponding theoretical function can be found with Eqs. (10), (11) and (21)

$$G_\rho^{th}(\mu) = 2.3 \cdot 10^{-2} (A_{rnd} \sigma_m)^3 \sqrt{\mu}, \quad (28)$$

and it is closely linked with the function $\sigma_m(\mu)$ and the power spectrum (5). For the standard power spectrum [68] $\sigma_m(\mu)$ is given by (11) and we get from (28)

$$G_\rho^{th}(\mu) \simeq \frac{0.6 A_{rnd}^3 \mu^{0.32}}{(1 + 1.8 \mu^{0.23})^3}. \quad (29)$$

As is shown on Fig. 2, the maximal value of the function (29) is achieved for $\mu_{max} \sim 0.05 - 0.1$, $M_{max} \sim (1 - 5) \cdot 10^{12} M_\odot$ and required amplitude is $A_{rnd} \simeq 3.5$. Similar results are obtained for the function $\sigma_m(\mu)$ presented in [62]. These functions are plotted in Fig. 2 (bottom panel).

Differences between the observed function $G_\rho^{obs}(\mu)$ and theoretical one $G_\rho^{th}(\mu)$ can be reduced by increasing the observed virial mass of galaxies (by a factor ~ 10). It also can be reduced by deformation of the power spectrum $P(k)$ (5). Deformation of both the initial power spectrum and the transfer function $T(kl_0)$ (6) also can be considered. The large scale power spectrum is measured by observations of the relic microwave radiation [6, 7]. So, here we assume that the power spectrum differs from

(5) by a correction function

$$\psi_{cor}(q) = 1 + \frac{q^2}{1 + a_c q^2}, \quad q = kl_0, \quad a_c \simeq 0.2. \quad (30)$$

This function increases the amplitude of the small scale power spectrum by the factor of $1/a_c$ and retains its shape. For so corrected power spectrum we have

$$\sigma_m(\mu) \simeq \frac{5\mu^{-0.066}}{1 + 3\mu^{0.31}} \quad (31)$$

and for the reduced virial density

$$G_\rho^{th}(\mu) \simeq \frac{5A_{rnd}^3 \mu^{0.3}}{(1 + 3\mu^{0.31})^3}. \quad (32)$$

As is seen from Fig. 2 observed (27) and corrected theoretical function (32) are similar to each other for the amplitude $A_{rnd} \sim 2$.

This approach is more sensitive for the small scale power spectrum but its reliability is yet not very high. Indeed, it is based on a limited statistic, observations are performed with limited precision, the theoretical base is the phenomenological PS model. Non the less these results confirm that for galaxies and clusters of galaxies the correlation of the virial density and the virial mass can be a natural result for the corrected power spectrum (5,30). One would expect that this approach can be used as a test of models of inflation [99, 100], and, in particular, it favors more complex models of inflation. It also allows to restrict parameters of WDM models and properties of hypothetical exotic DM particles [19, 46, 47].

Similar links between the halos masses and sizes are found for 160 systems of metal lines observed in absorption spectra of quasars [4], for 30 massive clusters in simulations [101] and for three clusters of galaxies at $z \simeq 0.4$ [87]. However for simulated low mass halos the reduced virial density is much smaller than (27). Thus for both halos associated with the 10^3 Ly- α absorbers [4] and $\sim 10^6$ low mass simulated halos [5] we get that

$$\langle G_\rho^{sim} \rangle \leq 2 \cdot 10^{-2}.$$

Simulations demonstrate [5] that for redshifts $z \leq 10$ the reduced density G_ρ of low mass halos is a many-valued function of the mass. This means that either these halos are not virialized, or the virial density is not described by the function (21) and, as it was discussed in Sec. 4.1, we need to use a more complex correction function, for instance, by inclusion z_{cr} – the redshift of halos formation. After such correction the many-valued character of the simulated virial density gets reasonable explanation: halos with the same μ are formed with the same $A_{rnd} D(z_{cr})$ (10,35,36) but different z_{cr} , ρ_{vir} and G_ρ . These expectations can be easy tested in simulations. For observed galaxies and clusters of galaxies such ambiguity is not so evident owing to the limited number of observed halos.

This unexpected different properties of observed and simulated halos can be formulated as the *virial paradox*. It shows that there are at least two populations of DM halos with different evolution and different properties. One of them is formed at high redshifts $z \geq z_{thr} \simeq 10$ and is observed as galaxies, and the other is formed at small redshifts, $z \leq z_{thr}$ do not contain stars and is observed, in particular, as Ly- α forest and circum galactic halos [4]. This effect is closely linked with the *missing satellite* problem.

4.4 Evolution of massive halos

In the PS model formation of halos is determined by the condition (10) and usually the model is applied to describe evolution of the mass function (12) and the mean mass of halos (14).

For the minimal mass $M_{min} = 10M_{\odot}$ we get for the mean mass

$$\langle M(z) \rangle = \frac{5.5 \cdot 10^8 M_{\odot} x_{10}^{11.5}}{1 + 0.5x_{10}^{6.5} + 1.8x_{10}^{0.5}}, \quad x_{10} = \frac{10}{1+z}. \quad (33)$$

This function is plotted in Fig. 3. At small redshifts $1 \leq z \leq 10$ the mean mass of halos is

$$\langle M \rangle = 1.7 \cdot 10^{14} M_{\odot} \frac{1 \pm 0.2}{(1+z)^{4.5}}. \quad (34)$$

The mass of a separate halo with the random peak amplitude A_{rnd} can be found with Eqs. (10) and (11)

$$\mu \simeq \frac{1.6 \cdot 10^{-4} x^{17.3}}{1 + 12x^7 + x^{11.8}}, \quad x = \frac{7A_{rnd}}{1+z}. \quad (35)$$

For $z \gg 1$, $x \ll 1$ this expression is quite similar to (33) and for $x \geq 1$ it is similar to (34). As is seen from (35) for $x \ll 1$ we have

$$\mu \simeq \left[\frac{4A_{rnd}}{1+z} \right]^{17}. \quad (36)$$

In these expressions the crucial role of the redshift $z \simeq 10$ is clearly seen since then the rate of matter concentration in the massive halos strongly changes. In turn, this change of the evolutionary rate is the direct result of the complex shape of the power spectrum (5),

$$(kl_0)^3 P(kl_0) \propto \begin{cases} \ln^2(kl_0) & kl_0 \gg 1, \\ (kl_0)^4 & kl_0 \ll 1. \end{cases} \quad (37)$$

These results are illustrated in Fig 3.

The PS model with a small minimal mass shows that already during the early period of evolution DM halos can accumulate significant mass fraction and it rapidly increases with time. Thus for the minimal mass $M_{min} =$

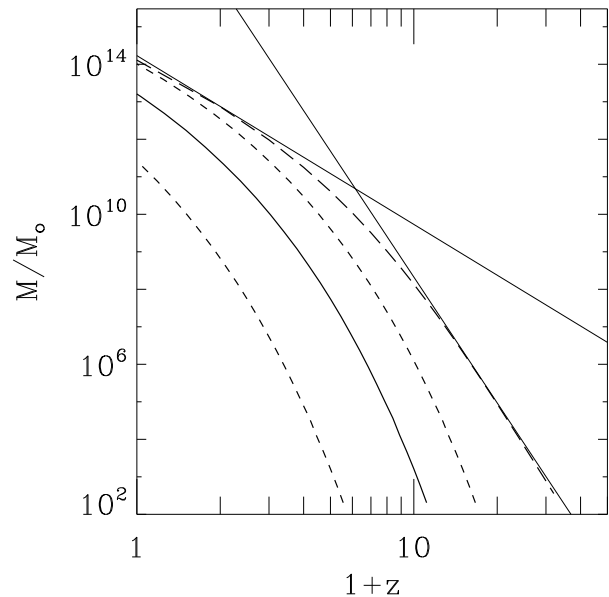


FIG. 3: The mass of DM halo (35) for amplitudes $A_{rnd} = 0.5, 1, 1.5$ are plotted vs. redshift by dashed and solid lines. Mean mass of the DM halos $\langle M(z, M_{min}) \rangle$ (33) is plotted by long dashed line. Thin straight lines plot the power fits (33).

$10^{-2}M_{\odot}$ at $z \simeq 50$ the matter fraction $f_m \sim 0.1$ is already concentrated in halos with $\langle M \rangle \simeq 0.2M_{\odot}$, and at $z \simeq 25$ the matter fraction $f_m \sim 0.3$ is accumulated in halos with $\langle M \rangle \simeq 10^3M_{\odot}$. At $z \simeq 10$ the matter fraction $f_m \sim 0.5$ is concentrated in halos with $\langle M \rangle \sim 10^8M_{\odot}$, but majority of DM is concentrated in less massive halos. At the same time halos with masses $M \geq 10^6M_{\odot}$, $\langle M \rangle \sim 10^9M_{\odot}$ accumulate only $f_m \sim 0.1$ but in such halos the first stars are formed, and they are responsible for reionization and reheating.

There are five natural consequences of the patch like model of galaxy formation and identification of galaxies with the highest density peaks:

1. At high redshifts $z \geq 10$ rapid ($M \propto (1+z)^{-17}$ (36)) regular growth of the central halo is accompanied by formation of many subhalos in the immediate vicinity of the central peak and their rapid merging.
2. During this period densities of the central halo and merged subhalos are similar and the shapes of subhalos are far from spherical [53]. These peculiarities allow to consider this medium as a mixture of collisionless dispersed DM particles and collisional irregular DM subhalos.
3. Rapid infall of surrounding subhalos into the central halo and their tidal disruption just after merging partly transforms the dissipationless evolution of the dispersed DM into the dissipational one of subhalos. Impact of the low entropy baryons amplifies this effect.

4. Accretion of the diffuse DM particles leads to formation of a cusp-like density profile (see, e.g., [33, 34, 66]), but successive merging of surrounding DM subhalos rapidly increases the central halo and gradually makes its cusp more and more shallow [1–3, 48, 49].
5. Accretion of the collisional fraction – DM subhalos – increases concentration of DM in the central core of halos and promotes formation of massive and supermassive central black holes.

These comments clarify qualitative differences in evolution of DM halos at high and small redshifts. Weak traces of these processes are seen in the present day simulations and are discussed in [12, 17]. More accurate quantitative estimates could be obtained from suitable simulations such as [3, 34, 49, 53].

For the later period ($z \leq 5$) of evolution growth of halos mass slows down (34) and there is a large gap between formation of massive clusters of galaxies at $z \simeq 1$ and high density galaxies at $z \geq 2$. In contrast with the high redshift evolution, collisions and striping of galaxies are rare, and in the observed clusters both the cusp like density profile and distinct high density galaxies could survive.

4.5 Evolution of the central cusp

At present the structure and evolution of the core of DM halos remains unclear as it can not be described analytically and in simulations it is investigated at high and low redshift in [1–3, 34, 102–104].

At $z \leq 10$ modern high resolution simulations provide a set of representative DM halos ranging from dwarf galaxies and up to rich clusters of galaxies. Their profile is found to be cusp-like and close to the two parametric Navarro-Frenk-White (NFW) profile [33]

$$\rho_{NFW}(r) \simeq \frac{\rho_0}{x^\alpha(1+x)^2}, \quad x = r/r_0, \quad \alpha = 1. \quad (38)$$

This profile reproduces reasonably well that observed for majority of clusters of galaxies. However in less massive galaxies the observed density profile is more shallow (Table I) and can be approximated by power law with the index $\alpha \leq 1$. Strong influence of random factors for galaxies manifests itself as larger scatter of the power index α . A review of observations is presented in [35]. More detailed discussion of this problem can be found in [15, 105–108] and references therein.

Now four models of flattening of the central cusp are discussed:

1. The most popular explanation is the cusp destruction owing to sudden removal of gas from the center of a cuspy DM halo caused by energy injection by explosions of supernovae [38].

TABLE I: Parameters of observed density profile

N_{obj}	$\alpha_{mn} \leq \alpha \leq \alpha_{max}$	$\langle \alpha \rangle$	reference
20 clusters	$0.5 \leq \alpha \leq 1.5$	1.02 ± 0.08	[109]
26 galaxies	$0 \leq \alpha \leq 1.2$	0.2 ± 0.2	[110]
15 galaxies	$0 \leq \alpha \leq 1.2$	0.6 ± 0.35	[111]
7 galaxies	$0 \leq \alpha \leq 1.2$	0.29 ± 0.07	[112]
26 galaxies	$0 \leq \alpha \leq 1.2$	0.32 ± 0.24	[113]
7 galaxies	$0.5 \leq \alpha \leq 0.73$	0.67 ± 0.10	[114]

2. In [40–43] the authors consider progressive destruction of the DM cusp owing to its tidal interaction with gaseous clouds, first stars and protostars.
3. In [44] the cusp erosion is related to accretion of a suitable DM spherical shell.
4. Models with exotic particle physics are presented in [19, 46, 47].

Of course, these factors influence the density profile but they are of secondary importance with moderate efficiency which depends upon thermal evolution of baryons, star formation or high energy physics. Recent discussion of this problem [16, 45] confirms the critical role of the threshold of stars formation and insufficient variety of mass profiles. Authors of [16, 45] believe that their simulations cannot explain the observed diversity of galactic rotation curves.

However, these inferences relate to simulations with the cutoff of power spectrum which cannot represent the earlier stage of halos formation responsible for the structure of the central region. It can be expected that matter compression went through a pancake-like anisotropic stage and the final density profile is formed by a complex relaxation processes.

In [53] these problems have been analyzed in detail using simulations at redshifts $0 \leq z \leq 3$ and the Minimal Spanning Tree technique. The main results of this investigation can be formulated as follow:

1. the shape of a halo with mass M is elliptical with half axes a_i and the velocity dispersion w_i

$$a_1 : a_2 : a_3 \sim (6 : 2 : 1)\sqrt{M}, \quad w_i \propto \sqrt{M}, \quad (39)$$

2. in accordance with the tidal torque theory [71–73] the angular momentum of clouds can be approximated by $|\mathbf{J}| \simeq 0.17|w_i|R_{vir}$ with the exponential PDF.
3. the turbulent motions can be approximated by the angular momentum $|\mathbf{j}| \simeq 0.8|w_i|R_{vir}$ with the Gaussian PDF.

These results indicate limited applicability of the spherical approach [78, 79] and a high influence of velocities

for evolution of the central regions of DM halos. Some applications of the tidal torque theory are discussed in [74–77].

High efficiency of tidal interactions for flattening of the cusp was demonstrated in [40–43] where the cusp disruption is explained by absorption and tidal destruction of a suitable set of stars and protostars. High efficiency of merging of surrounding DM subhalos and tidal heating of the central cores are confirmed by simulations [1–3, 49, 64, 115]. These papers illustrate the crucial role of initial stages of halos formation for correct reproduction of structure of DM halos and, in particular, for successive transformation of the central cusp into a core. They demonstrate that

1. For the low mass DM subhalos the central cusp is steeper than in the NFW model.
2. The central cusp becomes shallower owing to rapid merging processes as the halos mass increases.
3. The simulated mass dependence of the power index can be roughly fitted as

$$\alpha \simeq 0.123 \log \left(\frac{M}{10^6 M_\odot} \right). \quad (40)$$

This expression [1] describes both the small α at $M \sim (10^6 - 10^9)M_\odot$ and $\alpha \sim 1$ for clusters with $M \sim 10^{14}M_\odot$.

The new technique [34] allows to combine large simulated box and large redshift interval and it promise a rapid progress in investigations of the cusp – core transformations.

4.6 The missing satellites problem

The missing satellites problem is formulated as a strong discrepancy between the number of observed satellites of the Milky Way ($\sim 30 - 40$ at distances $D \leq 1Mpc$) and the number of simulated DM subhalos around massive galaxies [116]. It can be reformulated as high difference between the matter fraction concentrated in luminous galaxies and in the DM halos ($\sim 70\%$). Estimates of [117] show that only moderate fraction of baryons,

$$\Omega_{lum} \simeq 0.20(1 \pm 0.2)\Omega_b, \quad (41)$$

is concentrated in luminous objects (stars, galaxies, clusters of galaxies).

The main difference between galaxies and DM halos is the presence or absence of stars, what reduces the discussion to the problem of formation of stars – or even first stars. The virial paradox discussed in Sec. 4.3 shows that here we have to deal with two different populations of halos and it is closely linked with the shape of the primordial power spectrum of density perturbations (37).

Observations of the ultra diffuse galaxies [27] suggest that there is continuous transition between these populations.

The matter fraction (41) related to galaxies is comparable with that accumulated by high density massive halos before reheating of the Universe when the temperature of the low density baryons was rapidly increasing from $\sim 1K$ up to $\sim 10^4K$. (Next problem is the topology of the reionization bubble network [118]). The high density fraction of baryons kept low entropy and there the first stars could have been formed. This means that we can consider the stars as the trademark of such halos. The multitude of low mass DM halos formed later do not contain neither the low entropy baryons nor stars.

Conversion of DM halos into the observed luminous galaxies is a very complex multistep process [14, 119–122] which can be described only phenomenologically. These complexities prevent discrimination between simulated galaxies and invisible DM halos [123]. Besides, papers [27–29] show some unexpected features of dwarf galaxies what emphasizes again a complex character of their evolution. The PS formalism reproduces the observed estimate (41) and confirms that the missing satellites problem is deeply linked with the virial paradox and the identification of galaxies and simulated DM halos.

As is illustrated in [124] metal production in dwarf galaxies is irregular and randomized. Present day simulations can reproduce these processes only phenomenologically with special assumptions. This means that the missing satellites problem requires more adequate simulations with restoration of the patch like formation of galactic counterparts and the reheating process.

5. CONCLUSIONS

In this paper we consider evolution of the Λ CDM cosmological model with a small damping scale. In this model the patch like character of halos formation leads to creation of two different populations of objects. The first population includes high density halos formed before reheating in immediate vicinity of high density peaks identified with galaxies. Such halos contain stars and low entropy baryons and are observed as galaxies. Low mass halos of the second population are formed after reheating and they do not contain stars and low entropy baryons. Some of them are observed as the Ly- α forest [4] and circumgalactic matter [31].

Evolution of the second population is investigated in many simulations. In contrast, evolution of the first population is presented only in a few simulations [1–3, 34, 48, 49]. For its description we have to use abilities of analytically extended Press–Schechter and Zel’dovich approaches. Such models allow to reveal the main specific features of halos evolution, to clarify differences in properties of these populations and to explain the virial paradox, the core – cusp and the missing satellite prob-

lems. As discussed in Sec. 4, properties of these two families of halos are determined by the shape of the initial power spectrum of density perturbations.

Thus the patch like model demonstrates that:

1. The rapid formation of many subhalos at $z \geq 10$ in the immediate vicinity of the rare high density peaks and their rapid merging just after formation leads to a very rapid growth of mass of the central halo (33–36) and Fig. 3.
2. Tidal interaction of irregular merged subhalos with the central cusp makes it more and more shallow, what allows to explain the core – cusp problem and accelerates formation of the central black hole. These inferences are consistent with simulations [1–3, 48, 49, 65].
3. The patch like model demonstrates strong differences between characteristics of populations of galaxies created before reheating and numerous population of low mass dark DM halos created later. The last population does not contain low entropy baryons and stars. This division explains the missing satellite problem.
4. The path like model explains the *virial paradox* – observed correlations of the density and mass of first population of halos – galaxies and clusters of galaxies [4, 5] and links it with the initial power spectrum of density perturbations.
5. This link allows to estimate the shape of the small scale power spectrum (Fig. 2) and to place new constrains on the parameters of DM particles, WDM models and models of cosmological inflation. This approach deserves further refined investigations in both observations and simulations.

Traces of these processes are revealed in present day simulations and are discussed in [12, 17]. However these simulations cannot adequately reproduce both the early and later periods of structure evolution as well as the reheating of the intergalactic matter. This means that for our analysis we have to use theoretical models. Results obtained in this way cannot be considered as an actual proof of declared inferences but they reveal new important factors, actions of which were underestimated in previous discussions. Further progress can be achieved with new massive observations of virial parameters of galaxies and with simulations that use a new approach [34].

Acknowledgments

The work is supported by the scientific group 41-2020 of Lebedev Physical Institute.

We wish to thank the anonymous referee for valuable suggestions and many useful comments.

APPENDIX: STATISTICAL CHARACTERISTICS OF THE ZEL'DOVICH THEORY.

The Zel'dovich approximation [50–52] correctly describes the early anisotropic period of matter condensation and formation of elements of the Large Scale Structure of the Universe – network of filaments and walls–superclusters (Zel'dovich' 'pancakes') [51, 55, 56, 61?]. At all redshifts these elements are formed in the course of mildly nonlinear self similar matter compression described by Eq. (15, 16).

The original Zel'dovich model describes the matter condensation with the deformation tensor. However, for the CDM models with a small scale cutoff of the power spectrum this approach has to be reformulated in terms of displacements of particles what allows to prevent singularities at $kl_0 \gg 1$ and to concentrate more attention on observed and simulated scales. This requires modification of the statistical description of these processes. These problems have been discussed in [51, 53, 55, 61, 70] and are shortly presented here.

As it follows from (16) for the relative of displacements ΔS_i we get

$$\Phi_{ij}(\mathbf{q}_1, \mathbf{q}_2) = \langle \Delta S_i(\mathbf{q}_1) \Delta S_j(\mathbf{q}_2) \rangle = 2\Psi_{ij}(0) - 2\Psi_{ij}(q_{12}),$$

$$\Delta S_i(\mathbf{q}) = S_i(\mathbf{q}) - S_i(-\mathbf{q}), \quad q_{12} = |\mathbf{q}_1 - \mathbf{q}_2|,$$

$$G_{11} = \Phi_{11}(q_1, q_1) = \frac{2}{3}[1 - G_1(2q_1) - 4q_1^2 G_2(2q_1)], \quad (42)$$

$$G_{12} = \Phi_{12}(\mathbf{q}_1, \mathbf{q}_2) = -\frac{8}{3}q_1^2 G_2(\sqrt{2}q_1), \quad |\mathbf{q}_1| = |\mathbf{q}_2|.$$

These relations and eq. (17) allow us to estimate the coefficient correlations of the orthogonal displacements for the spectra discussed in Secs. 3 & 4 as

$$r_{12} = r_{13} = r_{23} = G_{12}(q_1, q_2)/G_{11}(q_1, q_1) \simeq 2/3. \quad (43)$$

Structure characteristics of uncorrelated distribution function of displacements

According to Eqs. (15,16) the Zel'dovich approach describes the matter condensation in compact clouds, filaments and walls. In particular it allows to estimate the evolution of matter fractions associated with – walls W_w , filaments W_f , clouds W_{cl} and voids W_v . For illustration we can ignore correlations between orthogonal displacements $\Delta S_i \Delta S_k$, $i \neq k$ and to assume that the distribution function for these displacements is Gaussian

$$dW = \Phi(\xi_1, \xi_2, \xi_3) d^3 \xi = 0.75 \exp(-Q) d^3 \xi, \quad (44)$$

TABLE II: Matter fraction accumulated by clouds, filaments, walls and voids for different threshold amplitude ζ and coefficient correlations of orthogonal displacements κ

ζ	κ	W_{cl}	W_f	W_w	W_v
0	0	0.125	0.375	0.375	0.125
0.5	0	0.029	0.197	0.443	0.331
1	0	0.004	0.063	0.337	0.596
0	0.66	0.045	0.455	0.455	0.045
0.5	0.66	0.004	0.200	0.597	0.200
1	0.66	1.e-4	0.052	0.488	0.459

$$Q = (\xi_1^2 + \xi_2^2 + \xi_3^2)/2, \quad -\infty \leq \xi_3 \leq \xi_2 \leq \xi_1 \leq \infty,$$

and $\xi_i = D(z)\Delta S_i/q_i$.

According to Eq. (15) the matter fractions accumulated by structure elements are determined by a common threshold $\zeta \geq 0$ and we get for voids,

$$\zeta \geq \xi_1 \geq \xi_2 \geq \xi_3 \geq -\infty \quad W_v = 0.125(1 + e(\zeta))^3,$$

where $e(\zeta) = erf(\zeta)$ and for the distinct clouds, formed directly from a weakly perturbed matter

$$\infty \geq \xi_1 \geq \xi_2 \geq \xi_3 \geq \zeta, \quad W_{cl} = 0.125(1 - e(\zeta))^3.$$

The matter fractions accumulated by filaments, W_f , and walls, W_w , are determined by similar conditions

$$\infty \geq \xi_1 \geq \xi_2 \geq \zeta \geq \xi_3 \geq -\infty, \quad W_f = 3W_{cl} \frac{1 + e(\zeta)}{1 - e(\zeta)}$$

$$\infty \geq \xi_1 \geq \zeta \geq \xi_2 \geq \xi_3 \geq -\infty, \quad W_w = 3W_v \frac{1 - e(\zeta)}{1 + e(\zeta)}.$$

Evidently, $W_w + W_f + W_{cl} + W_v = 1$. Thus, for $\zeta = 0$ we get

$$W_w = W_f = 3/8, \quad W_{cl} = W_v = 1/8,$$

but for $\zeta \geq 0$ the symmetry is destroyed (Table II) – walls and voids accumulate dominant fraction of matter.

However as was shown in the first Zel'dovich paper [50] the size of high density multistream regions associated with walls exceeds the size determined by the condition $\zeta = 1$ by a factor $\sqrt{3}$. This means that the condition $\zeta \simeq 0.5$ more correctly describes the compressed matter fractions.

Structure characteristics of the correlated distribution functions of displacements

The impact of correlations of the orthogonal displacements leads to more cumbersome estimates and can be suitably analyzed numerically using 10^7 random realizations. The correlation coefficient κ depends upon the

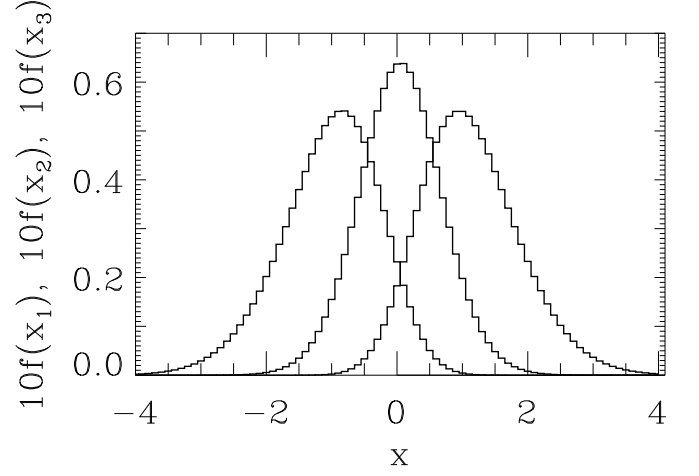


FIG. 4: The probability distribution functions for three displacements $\Delta S_1 \geq \Delta S_2 \geq \Delta S_3$ are plotted vs. $x = \Delta S_i/\sigma_i$, $\langle x_i \rangle = 1.07, 0, -1.07$, $\sigma_i = 0.76, 0.64, 0.76$.

power spectrum and for the power spectrum (5) $\kappa \sim 2/3$. For three amplitudes ζ the matter fractions accumulated by structure elements are presented in Table II

As is seen from this Table the matter fraction directly accumulated by clouds, W_{cl} is minimal, but for the amplitude $\zeta = 0.5$ the matter fraction accumulated by high density LSS elements, $1 - W_v$, increases up to 67% what is comparable with simulated results. As was shown in [125] and [126] after formation of high density filaments and walls they are rapidly disrupted into distinct relaxed clouds. This inference is also confirmed by simulations.

In the general case the PDF of the random displacements is Gaussian with correlation coefficients r_{ij} , $i, j = 1, 2, 3$, $-\infty \leq \xi_3 \leq \xi_2 \leq \xi_1 \leq \infty$

$$Q = \frac{\xi_1^2 + \xi_2^2 + \xi_3^2}{2} + \kappa_{12}\xi_1\xi_2 + \kappa_{13}\xi_1\xi_3 + \kappa_{23}\xi_2\xi_3, \quad (45)$$

$$\xi_i = \varepsilon_{jk}\Delta S_i, \quad \kappa_{ij} = \frac{r_{ij} - r_{ik}r_{jk}}{\sqrt{(1 - r_{ik}^2)(1 - r_{jk}^2)}}, \quad i \neq j \neq k,$$

$$\varepsilon_{jk}^2 = (1 - r_{jk}^2)/D, \quad D = 1 - r_{12}^2 - r_{13}^2 - r_{23}^2 + 2r_{12}r_{13}r_{23}.$$

As it follows from (43) for the spectra discussed in Sec. 3 & 4 we get

$$r_{ij} \simeq 2/3, \quad D \simeq 7/27, \quad \omega_{jk}^2 = 15/7, \quad \kappa_{ij} = 2/5.$$

These PDFs of the displacements are plotted in Fig. 4 and some numerical estimates are given in Table II.

To convert the expression (45) to the orthogonal form we use transformation

$$Q = \frac{1}{2}(\eta_1^2 + \eta_2^2 + \eta_3^2), \quad (46)$$

$$\xi_3 = \omega_{33}\eta_3, \quad \xi_2 = \omega_{22}\eta_2 - \omega_{23}\eta_3, \quad \xi_1 = \eta_1 - \kappa_{12}\xi_2 - \kappa_{13}\xi_3,$$

$$\omega_{33} = \sqrt{\frac{1 - \kappa_{12}^2}{DD}} \simeq 1.045, \quad \omega_{22} = \frac{1}{\sqrt{1 - \kappa_{12}^2}} \simeq 1.033,$$

$$\omega_{23} = \frac{\kappa_{23} - \kappa_{12}\kappa_{13}}{\sqrt{(1 - \kappa_{12}^2)DD}} \simeq 0.21,$$

where

$$DD = 1 - \kappa_{12}^2 - \kappa_{13}^2 - \kappa_{23}^2 + 2\kappa_{12}\kappa_{13}\kappa_{23} \simeq 27/32.$$

-
- [1] Ishiyama, T., 2014, ApJ, 788, 27
[2] Angulo, R., Hahn, O., Ludlow, A., et al., 2017, MNRAS, 471, 4667
[3] Delos, M., Bruff, M., Erickcek, A., 2019, 100b3523D
[4] Demiański, M., Doroshkevich, A., Larchenkova, T., 2020, ALet. 46, 359
[5] Demiański, M., Doroshkevich, A., Larchenkova, T., Pilipenko, S., 2020, ARep. 64, 883
[6] Komatsu, E., et al., 2011, ApJS, 182, 18
[7] Ade, P., Aghanim, N., Arnaud, M., et al., 2016, A&A, 594, 13
[8] Appleby, S., Park, C., Hong, S., Hwang, H., Kim, J. 2020, ApJ, 896, 145
[9] McQuinn, M., 2016, ARA&A, 1, 1
[10] Bullock, J., & Boylan-Kolchin, M., 2017, ARA&A, 55, 343
[11] Zasov, A., Saburova, A., Khoperskov, A., 2017, Phys.U, 60,3
[12] Naab, T., & Ostriker, J., 2017, ARA&A, 55, 59
[13] Tumlinson, J., Peebles, M., Werk, J., 2017, ARA&A, 55, 389
[14] Wechsler, R. & Tinker, J., 2018, ARA&A, 56, 435
[15] Salucci, P., 2019, A&ARv, 27, 2
[16] Bose, S., Frenk, C., Jenkins, A., et al. 2019, MNRAS, 486, 4790
[17] Zawala, J. & Frenk, C., 2019, Galaxies, 7, 81.
[18] Simon, J., 2019, ARA&A, 57, 375
[19] de Martino, I., Chakrabarty, S., Cesare, V., Gallo, A., Ostorero, L., Diaferio, A., arXiv:2007.15539
[20] White S., Rees, M., 1978, MNRAS, 183, 341
[21] White, S., & Frenk, C., 1991, ApJ, 379, 52
[22] Qu, Y., Helly, J., Bower, R., et al. 2017, MNRAS, 464, 1659
[23] Salcido, J., Bower, R., Theuns, T., 2019, MNRAS, in press, arXiv:1908.00552
[24] Guo, Q., White, S., Boylan Kolchin, M., et al. 2010, MNRAS, 404, 1111
[25] van den Bosch, F., Ogiya, G., Hahn, O., Burkert, A., 2018 MNRAS, 474, 3043
[26] Bahe, Y., Schaye, J., Barnes, D, et al., arXiv:1901.03336
[27] van Dokkum, P., Danieli, S., Cohen, Y., et al., 2018, Nature, 555, 629
[28] Oman, K., Navarro, J., Sales, L., Fattahi, A., Frenk, C., Sawala, T., Schallerr, M., White S., 2016, MNRAS, 460, 3610
[29] Guo, Q., Hu, H., Zheng, Z., et al., arXiv:1908.00046
[30] Bolton, J., Puchwein, E., Sijacki, D., et al., 2017, MNRAS, 464, 897
[31] Danforth, C., Keeney, B., Tilton, E., et al., 2016, ApJ, 817, 111
[32] Demiański, M.; Doroshkevich, A.; 2018, ARep. 62, 859
[33] Navarro J.F., Frenk C.S., & White S.D.M., 1995, MNRAS, 275, 720; 1996, ApJ, 462, 563; 1997, ApJ, 490, 493
[34] Wang, J., Bose, S., Frenk, C., Gao, L., Jenkins, A., Springel, V., White, S.D.M., 2020, Nature, 585, 39.
[35] de Blok W., 2010, Advances in Astronomy, 789293
[36] Pontzen, A., Governato, F., 2014, Nature, 596, 171
[37] Fernandez - Hernandez, L., Montiel. A., Rodrige-Meza, M., 2019, MNRAS, 488, 5127
[38] Navarro, J., Eke, V., Frenk, C., 1996, MNRAS, 283, L72
[39] Ceverino, D., Klypin, A., 2009, ApJ, 695, 292
[40] El-Zant, A., Freundlich, J., Combes, F., 2016, MNRAS, 461, 1745
[41] Del Popolo, A., Pace, F., 2016, Ap&SS, 361, 162
[42] Del Popolo, A., Le Delliou, M., 2017, Galax, 5, 17
[43] Del Popolo, A., Pace, F., Le Delliou, M., Lee, X., 2018, PhRvD., 98f3517D
[44] Freundlich, J., Dekel, A., Jiang, F., Ishai, G., Cornuault, N., Lapiner, S., Dutton, A., Maccio, A., 2019, arXiv:1907.11726
[45] Benitez-Llambay, A., Frenk, C., Ludlow, A., Navarro, J., 2019, MNRAS, 488, 2387
[46] Hui, L., Ostriker, J., Tremain, S., Witten, E., 2017, PhRvD, 95, 043541
[47] Bernal, T., Fernández-Hernández, L., Matos, T., Rodríguez-Meza, M., 2018, MNRAS, 475, 1447
[48] Delos, M., Erickcek, A., Bailey, A., Avarez, a., 2018, Phys.Dev.D., 97d1303D
[49] Delos, M., Erickcek, A., Bailey, A., Avarez, a., 2018, Phys.Dev.D., 98f3527D
[50] Zel'dovich, Ya., 1970, A&A, 5, 84
[51] Shandarin, S., Doroshkevich, A., Zel'dovich, Ya., 1983, Soviet Physics Uspekhi, 26, 46
[52] Shandarin, S., Zeldovich, Ya., 1989, RvMP, 61, 185
[53] Demiański, M.; Doroshkevich, A.; Pilipenko, S.; Gottloeber, S., 2011, MNRAS, 414, 1813
[54] Feldbrugge, J., van de Weygaert, R., Hiddingb, J., Feldbrugge, J., 2018, JCAP, 05, 027
[55] Doroshkevich, A.; Tucker, D.; Allam, S.; Way, M.; 2004, A&A, 418, 7
[56] Shandarin, S., 2020, arXiv:2005.14548
[57] Ishiyama, T., Prada, F., Klypin, A., et al., 2020, arXiv:2007.14720
[58] Press, W., Schechter, P., 1974, ApJ, 187, 425
[59] Bond, J., Cole, S., Efstathiou, G., Kaiser, N., 1991, ApJ, 379, 440
[60] Sheth, R., Tormen, G., 2002, MNRAS, 329, 61
[61] Demiański, M., Doroshkevich, A., 2004, A&A, 422, 423
[62] Klypin, A., Trujillo-Gomez, S., Primack, J., 2011, ApJ, 740, 102
[63] Bertschinger, E., 2006, Phys.Rev.D., 74f3509
[64] Drakos, N., Taylor, J., Berrouet, A., Botham, A., Power, C., 2019, MNRAS, 487, 1008
[65] Diemand, J., Moore, B., Stadel, J., 2005, Nature, 433, 389
[66] Anderhalden, D., & Diemand, J., 2011, MNRAS, 415, 2293
[67] Anderhalden, D., & Diemand, J., 2013, MNRAS, JCAP, 08, 002
[68] Bardeen J.M., Bond J.R., Kaiser N., & Szalay A., 1986,

- ApJ, 304, 15
- [69] Loeb, A., Zaldarriaga, M., 2005, PhRvD, 71j3520
- [70] Demiański, M., Doroshkevich, A., 1999, ApJ, 512, 527
- [71] Peebles, P., J.E., 1969, APJ, 155, 393
- [72] Doroshkevich, A., 1970, Astrophysics, 6, 320
- [73] White, S.D.M., 1984, ApJ, 286, 38
- [74] Lopez, P., Merchán, M., Paz, D., 2019, MNRAS, 485, 5244
- [75] Ganeshaiiah Veena, P.; Cautun, M.; van de Weygaert, R., Tempel, E, Frenk, C., 2018, MNRAS. 481. 414
- [76] Ganeshaiiah Veena, P.; Cautun, M.; van de Weygaert, R., Tempel, E, Frenk, C., 2019, MNRAS. 487. 1697
- [77] Ganeshaiiah Veena, P.; Cautun, M.; van de Weygaert, R., Tempel, E, Frenk, C., 2030, arXiv2007.10365
- [78] Fillmore J.A., & Goldreich P., 1984, ApJ, 281, 1
- [79] Gurevich, A., Zybin, K., 1995, Phys.Usp., 38, 687
- [80] Peebles, P., 1967, ApJ, 147, 859
- [81] Zeldovich, Ya., Kazhdan, Ya., 1970, Astrophysica, 6, 50
- [82] Lacey, C., & Cole, S., 1993, MNRAS, 262, 627
- [83] Landau, L., & Lifshitz, E., 1975, The classical theory of fields, Oxford: Pergamon Press
- [84] Bonamigo, M., Despali, G., Limousin, M. Angulo, R., Giocoli, C., Soucail, G., 2015, MNRAS. 449. 3171
- [85] Despali, G., Giocoli, C., Bonamigo, M., Limousin, M. Tormen, G., 2017, MNRAS, 466, 181
- [86] Balestra, J., Mercurio, A., Sartoris1,B., et al., 2016, ApJS, 224, 33
- [87] Bonamigo, M., Grillo, C., Ettory, S., et al, 2018, ApJ, 864, 98
- [88] Sheth, R., Tormen, G., 2004, MNRAS, 349, 1464
- [89] More, S., Miyatake, H., Takada, M., Diemer4, B., 2016, ApJ, ,825, 39
- [90] Libeskind N., et al., 2018, MNRAS, 473, 1195
- [91] Despali, J., Giocoli, C., Bonamigo, M., Limousin, M., Tormen, G., 2017, MNRAS, 466, 181
- [92] Bonamigo, M., Grillo, C., Etton, S., Caminha, G., Rosati, P., et al. 2018, ApJ, 864, 98
- [93] Connor, T., Kelson, D., Mulchaey, J., et al., 2018, ApJ, 867, 25.
- [94] Umehata, H., et al., 2019, Science, 366, 97
- [95] Vikhlinin, A., Kravtsov, A., Burenin, R., et al., 2009, ApJ, 692, 1060
- [96] Kelly, B., Vestergaard, M., Fan, X., et al., 2010, ApJ, 719, 1427
- [97] Decarli, R., Walter, F., Venemans, B., et al., 2020, ApJ., 854, 97
- [98] Onken, C., Bian, F., Fan, X., Wang, F., Wolf, C., Yang, J., 2020, MNRAS, 496, 2309
- [99] Hazra, D., Shafieloo, A., Smoot, G., Starobinskye, A., JCAP, 2014, PhRvL, 113g1301H
- [100] Ballardini, M., Braglia, M., Finelli, F., et al., arXiv:200414349
- [101] Armitage, T., Harnes, D., Kay, S., et al., 2018, MNRAS, 474, 3746
- [102] Diemer, B., Kravtsov, A., 2015, ApJ, 799, 108,
- [103] Diemer, B., Joyce, M., 2019, ApJ, 871, 16
- [104] Diemer, B., 2020, aeXiv:2007.10346
- [105] Borriello, A. Salucci, P. 2001 MNRAS, 323, 285
- [106] Salucci, P. 2001 MNRAS 320, 1
- [107] Gentile, G. Salucci, P. Klein, U. Vergani, D. Kalberla, P., 2004, MNRAS, 351,903
- [108] di Paolo, C., Salucci, P., Erkurt, A., 2019, MNRAS, 490. 5451
- [109] Mantz, A., Allen, S., Morris, R., 2016, MNRAS, 462, 681
- [110] de Blok, W., & Bosma, A., 2002, A&A, 375, 816
- [111] Swaters, R., Madore, B., van den Bosch, F., Balcells, M., 2003, ApJ, 583, 732
- [112] Oh, S-H., Brook, C., Governato, F., et al., 2011, AJ, 142, 24
- [113] Oh, S-H., Hunter, D., Brinks, E., et al. 2015, AJ, 149, 180
- [114] Adams, J., Simon, J., Fabricius, M., et al. 2014, ApJ, 789, 63
- [115] Penarrubia, J., 2019, MNRAS, 484, 5409
- [116] Klypin, A. Karachentsev, I., Makarov, D., Nasonova, O., 2015, MNRAS, 454, 1798
- [117] Shull, J., Smith, B., Danforth, C., 2012, ApJ, 759, 23
- [118] Elbers, W., van de Weygaert, R., 2019, MNRAS 486, 1523
- [119] Behroozi, P., Wechsler, R., Hearin, A., Conroy, C., 2018, arXiv:180607893
- [120] Goh, T., Primack, J., Lee, C., et al., 2019, MNRAS, 483, 2101
- [121] Allen, M., Behroozi, P., Ma, C. 2018, arXiv:181205733
- [122] Somerville, R., et al., 2018, MNRAS, 473, 2714
- [123] Sawala, T., Frenk, C., Fattahi, A., et al., 2016, MNRAS, 457, 1931
- [124] Weisz, D., Dolphin, A., Skillman, E., et al., 2014, ApJ, 789, 148
- [125] Sunyaev, R., & Zel'dovich, Ya., 1972, AĀ, 20, 189
- [126] Doroshkevich, A., 1980, SvA., 24, 152